J. Hydrol. Hydromech., 71, 2023, 3, 305–315
https://doi.org/10.2478/johh-2023-0005
©2023 Ibrahim Rahou et al., published by Sciendo. This work is licensed under the Creative Commons Attribution-NonCommercial-NoDerivatives 4.0 International Licence.

sciendo Journal of Hydrology and Hydromechanics Institute of Hydrology SAS

Comparative analysis of numerical solutions of 2D unsteady dambreak waves using FVM and SPH method

Ibrahim Rahou, Khaled Korichi*

Civil Engineering and Environment Laboratory, Faculty of Technology, Djillali Liabes University of Sidi Bel Abbes, Bp 89 Sidi Bel Abbes 22000, Algeria.
* Corresponding author. E-mail: kh.korichi@gmail.com

Abstract: This work presents a comparison of two-dimensional numerical solutions of unsteady free surface flow. This is a simulation of the dam-break wave with different configurations using based-mesh finite volume method and meshless smoothed particle hydrodynamics (SPH). Two well-known approaches, widely used in the computational fluid dynamics (CFD). These techniques have proven their robustness in the numerical treatment of such conservation laws. The main goal is to check the ability of the SPH method and the first order finite volume HLLC solver to reproduce the numerical solutions of the 2D shallow water equations. Based on many benchmark tests, one investigates the effect of the topographic variation along the x and y directions on behavior of the numerical solutions namely at the wet-dry front. The comparison between the simulated results, the analytical solutions and the experimental measurements shows a good correlation, although the finite volume approach remains more advantageous in terms of accuracy and the CPU time.

Keywords: 2D shallow water; Unsteady flow; Dambreak; Finite volume; SPH; Experimental measurements.

1 INTRODUCTION

Free surface and geophysical fluid flows are complex physical phenomena and represent an important class of problems encountered in rivers and oceans, such as floods and inundations, dam failure, tsunamis, tidal waves, and pollution diffusion.

The basic equations governing one-dimensional, non-stationary, gradually, and rapidly varying free surface flows were at first formulated in 1871 by Claude Barré de Saint-Venant (Saint-Venant, 1871).The mathematical model of Saint-Venant (SVE), valid in shallow environments, represents a system of nonlinear and hyperbolic partial differential equations (PDE) which is derived from the principles of conservation of mass and conservation of momentum under certain assumptions such as: 1) Smooth slope channel bottom, 2) Uniform velocity along the cross-section, 3) Steady-state friction laws are valid to unsteady flow, 4) Incompressible fluid and 5) Hydrostatic distribution of the pressure (Cunge et al., 1980).

Another technique is used to describe 2D flows by integrating the Navier-Stokes equations along the flow depth. The resulting equations are also two-dimensional nonlinear (PDEs) that describe the evolution of the flow depth and the mean fluid velocity (Chaudhry, 2008).

Mathematical models can be written in either integral or differential form. However, the differential form requires sufficient regularity of the solutions and hence oscillates near discontinuities. Therefore, the conservation equations must be expressed correctly in their integral form. Since the PDE system is hyperbolic, discontinuities appear, especially shock waves in the majority of flow problems such as hydraulic jumps. These waves can develop spontaneously, even from regular initial data, which requires mathematical and numerical treatment (LeVeque, 2002). Due to the non-linearity of the mathematical model, it is very difficult to find an exact and unique analytical solution except under simple and typical situation (Delestre et al., 2016).

Numerical modeling of the shallow water equations (SWE) is confronted with numerous problems which are generally the source of the instability and the low accuracy of the numerical solutions, in particular in the simulation of the problems characterized by strong discontinuities and by complex geometry, as well as in the presence of wet/dry interfaces (Ríha et al., 2019). In such cases: 1) the SWE system admits discontinuous solutions, and therefore requires a robust numerical scheme that accurately captures the shocks. 2) Simple stationary solutions; such as subcritical (tranquil) flow in complex geometry, must be calculated correctly. Therefore, the numerical scheme must satisfy the equilibrium condition or C-property (Bermudez and Vazquez, 1994). That means; the discretization approaches for the flux term and the source terms (topography and friction) must ensure an appropriate balance. 3) In dry areas (e.g. flooding or drainage flows) the water depth cancels out and the system loses its hyperbolicity, some numerical schemes then produce negative depth values or non-physical high velocities (Yang et al., 2022). Many numerical approaches have been proposed in the literature to deal with dry/wet problems and preserve the positivity of the water depths at all points and at all time (Bunya et al., 2009).

In terms of the domain discretization, two classes of numerical methods are used; mesh-based methods and meshless methods. Mesh-based methods are the most commonly used approaches for approximating the numerical solution; such as the method of characteristics (Abbott et al., 1984), finite difference method (FDM) (Molls and Chaudhry, 1995), finite element method (FEM) (Li and Liu, 2001) and the finite volume method (FVM) (Yoon and Kang, 2004).

Recently and with the great progress of computer technology, several research works based on various codes have been developed and adapted to simulate shallow water flows such as HEC-RAS (Brunner, 2018), MIKE-FLOOD (Danish Hydraulic Institute DHI, 2014), SOBEK (Deltares Systems, 2019), TELEMAC-2D (Hervouet and Ata, 2017), LISFLOOD-FP (LISFLOOD-FP Developers, 2020), TUFLOW-FV (BMT & WBM, 2014), ANUGA Hydro (Roberts et al., 2015), CLAWPACK (Mandli et al., 2016) and BASEMENT (Vetsch et al., 2022).

The most popular and widely used numerical method among those mentioned above is the finite volume method. This method combines, on the one hand, the geometric flexibility of the FEM and on the other hand, the conceptual simplicity of the FDM (Mingham and Causon, 1998).

The finite volume method is based on the discretization of the integral form rather than the differential form of the shallow water equations (SWE) into a certain number of elementary volumes (also called cells), which ensures the local mass and momentum conservation. The global conservation is then checked if the boundary conditions are correctly imposed. At each time step, the fluxes at the cell interfaces are calculated and thus update the conservative variables stored at the center of each cell. The main challenge of this method consists in finding the numerical flux functions which result in an accurate approximation of the fluxes (LeVeque, 2002).

The nature of the numerical scheme is defined by the way the numerical flux is approximated. There are mainly two types of discretization schemes: the centered schemes and the upwind schemes. The upwind schemes calculate the fluxes at the cell interfaces based on the direction of the convection velocity and therefore use values which correspond to the origin of the characteristics, whereas this characteristic direction is ignored in the central schemes since they are based on local flux calculations and use a symmetric discretization (Hirsch, 1988).

Godunov's scheme (Godunov, 1959) is a popular first-order finite volume upwind-type scheme and it has been originally proposed to solve the nonlinear Euler equations of gas dynamics. The fluxes are approximated at cell interfaces by a piecewise constant function to solve the Riemann problem. Many approximate solvers, based on the characteristic theory, were later proposed to replace the Riemann solver, such as: Flux Difference Splitting (FDS), Roe's solver (Roe, 1981), Flux Vector Splitting (FVS), Steger & Warming solver (Steger and Warming, 1981), Osher and Solomon solver (Osher and Solomon, 1982), Harten HLL solver (Harten et al., 1983), HLLC solver (Toro et al., 1994). These solvers are also applied to solve shallow water equations in several works (Alcrudo et al., 1992; Glaister, 1988; Mingham and Causon, 1998; Nujić, 1995; Zhao et al., 1994; Zoppou and Roberts, 1999).

Unlike mesh-based approaches, meshless methods do not use a grid to discretize the space domain. There are several approaches in particular those based on particles, such as the SPH method (Smooth Particle Hydrodynamics), the MPS method (Moving Particle Semi-implicit method), the RKPM method (Reproducing Kernel Particle Method) and the DPD (Dissipative Particle Dynamics method).

The SPH method has caught the attention of many scientists and researchers and it is now the most popular meshless method used in the literature due to its excellent ability to reproduce interface motions, large deformations, and flow problems in mobile boundaries (Liu and Liu, 2003). The SPH method was applied for the first time to simulate phenomena related to the astrophysics (Gingold and Monaghan, 1977; Lucy, 1977). Later, it was applied to predict free surface flows by solving the Navier-Stokes equations (Monaghan, 1994).

As a purely Lagrangian method; 1) it conserves exactly the mass; 2) the nonlinear convection terms will not be present in the solved equations; 3) the wet/dry interface can be described automatically without a special treatment (Monaghan, 2005). These advantages make the SPH method more attractive for simulating problems related to shallow waters such as; the pollution diffusion, two-phase flow, bedload, etc. (Gu et al., 2017), as well as for the development of several codes such as GPUSPH (Herault et al., 2008), DualSphysics (Dominguez et al., 2021), and SWE-SPHysics (Vacondio et al., 2011).

In the present work, the main purpose of the simulation is to estimate the arrival time of the dambreak waves, which represents a decision-support tool to install an alert system to protect the inhabitants downstream the dams. Following recent advances in the field, we carry out a comparative study of the numerical solutions of the shallow water equations between the HLLC finite volume method and the SPH method. Both approaches will be examined in terms of accuracy, stability, efficiency, robustness, and the CPU time of simulation. For this purpose, one uses the finite volume BASEMENT models and SWE-SPHysics which is based on the SPH approach to simulate various types of flow: subcritical and supercritical and unsteady. The numerical results are also compared with the analytical solutions and experimental data.

2 METHODOLOGY

2.1 Mathematical model

The equations that govern shallow water flows form a nonlinear and hyperbolic (PDE) system. The 2D model can be written in its vector and conservative form as:

$$\frac{\partial U}{\partial t}+\frac{\partial F_x(U)}{\partial x}+\frac{\partial F_y(U)}{\partial y}=S(U) \tag{1}$$

In which U, $F_x(U)$, $F_y(U)$ and $S(U)$ are respectively the vectors of conservative variables, the fluxes in the directions x and y and the source terms which represent the effects of the topography and the friction such as:

$$\boldsymbol{U}=\begin{pmatrix} h \\ uh \\ vh \end{pmatrix};\ \boldsymbol{F_x}(\boldsymbol{U})=\begin{pmatrix} uh \\ u^2h+\frac{1}{2}gh^2 \\ uvh \end{pmatrix};$$

$$\boldsymbol{F_y}(\boldsymbol{U})=\begin{pmatrix} vh \\ uvh \\ v^2h+\frac{1}{2}gh^2 \end{pmatrix} \tag{2}$$

$$\text{and } \boldsymbol{S}(\boldsymbol{U})=\begin{pmatrix} gh\left(-\frac{\partial z_b}{\partial x}-\frac{n^2u\sqrt{u^2+v^2}}{h^{4/3}}\right) \\ gh\left(-\frac{\partial z_b}{\partial y}-\frac{n^2v\sqrt{u^2+v^2}}{h^{4/3}}\right) \end{pmatrix}$$

where u and v (m s^{-1}) are the mean velocity components along the x and y direction, respectively, h (m) is the water depth (cf. Figure 1), z_b(m) is the bottom elevation, n is Manning's roughness coefficient (m$^{-1/3}$ s), g is the acceleration due to gravity (m s^{-2}).

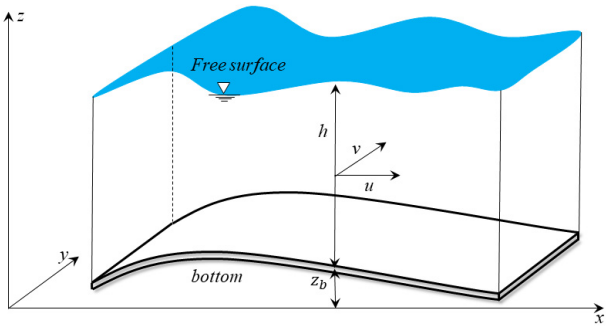


Fig. 1. Definition sketch of the SWE's parameters.

2.2 Numerical methods

2.2.1 Finite volume solver for SWE

Finite volume discretization ensures that mass and momentum are conserved across the cell interfaces. By integrating Equation (1) into the cell $\mathbf{V} = [\Omega_i] \times [t_n, t_{n+1}]$ and taking both the conserved variables and the source terms to be constants across the cell area Ω_i, we can write:

$$\boldsymbol{U}_i^{n+1} = \boldsymbol{U}_i^n - \frac{\Delta t}{|\Omega_i|}\sum_{j=1}^{3} (\boldsymbol{F}, \boldsymbol{G})_{i,j}^n \cdot \boldsymbol{n}_{ij} l_{ij} + \Delta t \boldsymbol{S}_i \quad (3)$$

where the exponent n indicates the time step, i, j represent respectively the cells indices, Δt is the time step, l_{ij} is the length of the common interface Γ_{ij} between two neighboring cells Ω_i and Ω_j (cf. Figure 2), $\boldsymbol{n}_{ij} = (\boldsymbol{n}_{ij,x}, \boldsymbol{n}_{ij,y})$is the unit vector which is normal to the edge Γ_{ij} and pointed to the cell Ω_j, $(\boldsymbol{F}, \boldsymbol{G})_{ij}$ are the estimated hydrodynamic flux vectors at the cell interface and $\boldsymbol{S}_i$ represents the source terms vector of both friction and slope.

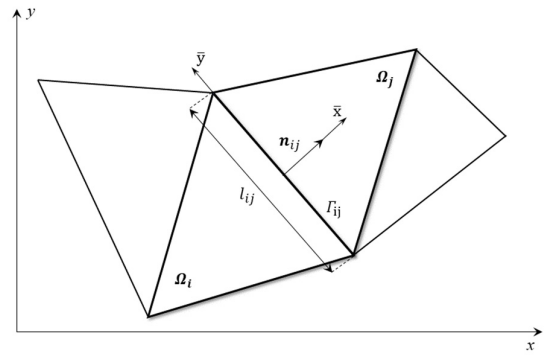


Fig. 2. Simplified unstructured triangular mesh.

The resulting Equation (3) represent a first order Godunov type scheme. In this work, The Riemann problem is solved at each interface adopting the Harten-Lax-Van Leer-Contact (HLLC). The approximate Riemann HLLC solver estimates the velocities of the left and right waves and also the central wave (contact discontinuity) (cf. Figure 3) which splits two constant states.

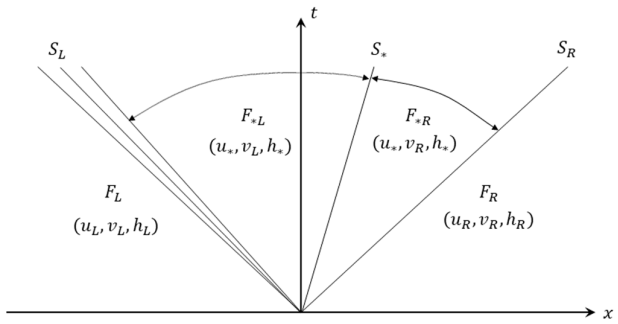


Fig. 3. Structure of HLLC solver of a Riemann problem.

The numerical flux in the interface is given by:

$$F_{i+1/2} = \begin{cases} F_L & if \quad 0 \le S_L, \\ F_{*L} = F_L + S_L(U_{*L} - U_L) & if \quad S_L \le 0 \le S_*, \\ F_{*R} = F_R + S_R(U_{*R} - U_R) & if \quad S_* \le 0 \le S_R, \\ F_R & if \quad 0 \ge S_R. \end{cases} \quad (4)$$

where $F_L = F_L(U_L)$ and $F_R = F_R(U_R)$ are determined from the left and right Riemann states U_L and U_R. The fluxes F_{*L} and F_{*R} represent respectively the left and right states of the central contact wave. S_L, S_* and S_R are respectively the estimated wave velocities for the left, center and right states. For more details, the reader can refer to Toro's works (Toro, 2001).

The discretization of the source terms $\boldsymbol{S}(U)$ in Equation (2) is carried out separately, according to the nature of each term. The numerical treatment of the bed slope term is formulated based on Komaei's method (Komaei and Bechteler, 2004) to ensure the C-property and then is updated using the forward values $\boldsymbol{U}_i^{n+1/2}$. The friction term is discretized using semi-implicit scheme.

This model is a second-order temporal scheme subject to the CFL (Courant-Friedrichs-Lewy) criterion, which limits or adapts the time step. In the case of the 2-D model, the number of Courant is defined as follows:

$$CFL = \frac{\left(\sqrt{u^2 + v^2} + c\right)\Delta t}{L} \quad (5)$$

where L is the cell interface length and the celerity $c = \sqrt{gh}$. The HLLC scheme is stable for $0 < CFL \le 1$.

2.2.2 SPH solver for SWE

To adapt the SWE model to the SPH treatment we have to use a Lagrangian version of the SWE model rather than the Eulerian as follows:

$$\frac{\mathrm{d}\rho}{\mathrm{d}t} = -\rho \nabla \cdot \mathbf{v} \quad (6)$$

$$\frac{\mathrm{d}\mathbf{v}}{\mathrm{d}t} = -\frac{\rho}{\rho_w}\nabla\rho + g\left(\nabla z_b + \mathbf{S}_{fr}\right) \quad (7)$$

where $\rho = \rho_w h$, ρ is the mass of fluid per unit area in (2D) domain, ρ_w is the constant three-dimensional (3D) (conventional) density and h is the water depth (Rodriguez-Paz and Bonet, 2005), $\mathbf{v}(u, v)$ is the depth-average velocity vector, u and v (m s^{-1}) are its components in the x and y directions, respectively, (cf. Figure 4), z_b(m) is the bottom elevation, and $\boldsymbol{S}_{fr}$ is the bed friction source term.

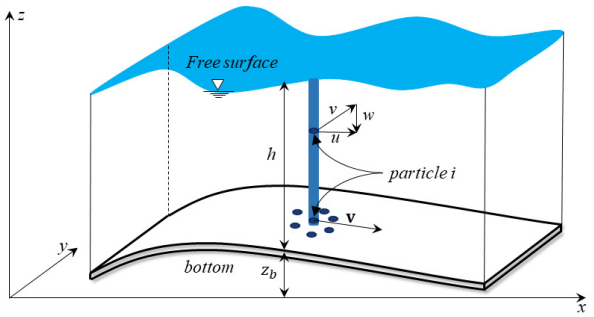


Fig. 4. Definition sketch of the SWE's parameters (SPH version).

In the present study, the density (converted to water depth) of each particle is calculated by the summation operator SPH such as:

$$\rho_i = \sum_j m_j W_i\left(\mathbf{x}_j, h_{sm,i}\right) \quad (8)$$

where m_j is the mass of particle j and $W_i(\mathbf{x}_j, h_{sm,i})$ is the cubic spline kernel (Liu and Liu, 2003). The smoothing length $h_{sm,i}$ is related to the density according to (Benz, 1990):

$$h_{sm,i} = h_{sm,0}\left(\frac{\rho_0}{\rho_i}\right)^{\frac{1}{d_m}} \tag{9}$$

in which ρ_0 is the initial density of the particle i, ($h_{sm,0} = 1.2\Delta x_0$ in 1D and $h_{sm,0} = 1.2 \times 0.5 \times (\Delta x_0 + \Delta y_0)$ in 2D), and d_m is the number of the space dimensions (1 if 1D and 2 if 2D).

Following the work of (Rodriguez-Paz and Bonet, 2005), the momentum Equation (7) can be approximated using a variational approach. As a result, the approximate momentum equations, that automatically give the discrete conservation laws, are expressed as follows:

$$\left(\frac{\mathrm{d}\mathbf{v}}{\mathrm{d}t}\right)_i = \frac{g + \mathbf{v}_i \cdot \mathbf{k}_i \mathbf{v}_i + \mathbf{t}_i \cdot \nabla z_{b,i}}{1 + \nabla z_{b,i} \cdot \nabla z_{b,i}} \nabla z_{b,i} - \mathbf{t}_i + \boldsymbol{S}_{fr,i} \tag{10}$$

in which $\nabla z_{b,i}$ is the bottom elevation gradient, $\boldsymbol{k}_i = \nabla(\nabla z_{b,i})$ is the curvature tensor of $z_b(x, y)$. It is derived using the integral approximation of (Monaghan, 2005), $\boldsymbol{S}_{fr,i}$ is the source term due to friction and $\mathbf{t}_i = \mathbf{T}_i/m_i$ is the acceleration due to internal forces $\mathbf{T}_i$. It is given by the SPH formulation as (Bonet and Lok, 1999):

$$\mathbf{T}_i = \sum_j m_i m_j \left(\frac{p_j}{\alpha_j \rho_j^2} \nabla W_j(\mathbf{x}_i, h_{sm,j}) - \frac{p_i}{\alpha_i \rho_i^2} \nabla W_i(\mathbf{x}_i, h_{sm,i}) \right) \tag{11}$$

where p is the hydrostatic pressure, $p = \frac{1}{2}\rho_w g h^2$, α is the correction factor due to the variation of the smoothing length defined as:

$$\alpha_i = -\frac{1}{\rho_i d_m} \sum_j m_j r_{ij} \frac{dW_{ij}}{dr_{ij}} \tag{12}$$

where r_{ij} = distance between the particles i and j.

To avoid numerical oscillation in the presence of shock waves, one adds an artificial viscosity.Π_{ij}, the Equation (11) becomes:

$$\mathbf{T}_i = \sum_j m_i m_j \frac{g}{2\rho_w} \left[\left(\frac{1}{\alpha_j} + \Pi_{ij} \right) \nabla W_j(\mathbf{x}_i, h_{sm,j}) - \left(\frac{1}{\alpha_i} + \Pi_{ij} \right) \nabla W_i(\mathbf{x}_i, h_{sm,i}) \right] \tag{13}$$

In this study, the Lax-Friedrichs stabilization term Π_{ij} (Ata and Soulaïmani, 2005) is used. The process of the Monotone Upwind-Centred Scheme for Conservation Laws (MUSCL) (Edwards, 2006) is adopted as a minmod-type slope limiting function to reduce the numerical viscosity and to increase the accuracy of the SPH interpolation (Toro, 2001).

The bed elevation source term discretized using the SPH interpolation is performed by a new set of fixed particles. These particles are used only to describe the bathymetry. The elevation $z_{b,i}$ of the fluid particles is calculated as follows:

$$z_{b,i} = \sum_j z_{b,j} \overline{W}_i(\mathbf{x}_i - \mathbf{x}_j^b, h_{sm,j}^b) V_j \tag{14}$$

where $\mathbf{x}_j^b$, $h_{sm,j}^b$, $z_{b,j}$ and V_j are respectively the position, smoothing constant length, bottom elevation and volume of the j-th bottom particle. $\overline{W}_i$ is the kernel for the i-th particle corrected using the Shepard filter(Shepard, 1968).The gradient of the bottom elevation $\nabla z_{b,i}$ is evaluated using an SPH interpolation as:

$$\nabla z_{b,i} = \sum_j z_{b,j} \widetilde{\nabla} W_i(\mathbf{x}_i - \mathbf{x}_j^b, h_{sm,j}^b) V_j \tag{15}$$

where $\widetilde{\nabla} W_i$ is the corrected kernel gradient as proposed in Bonet and Lok (1999).The bed friction source term $\boldsymbol{S}_{fr,i}$ for each particle i-th can be written as:

$$\boldsymbol{S}_{fr,i} = \mathbf{v}_i \frac{g n_i^2 |\mathbf{v}_i|}{h_i} \tag{16}$$

where n_i is Manning's coefficient. It is calculated at each time step by the SPH interpolation as:

$$n_i = \sum_j n_j^b \overline{W}_i(\mathbf{x}_i - \mathbf{x}_j^b, h_{sm,j}^b) V_j \tag{17}$$

n_j^b = Manning's coefficient of the j-th bed particle located at $\mathbf{x}_j^b$. The closed boundaries (walls) are simulated using the modified virtual boundary particle method (Vacondio et al., 2011).

The time integration of the particle positions and the velocities is done according to the leap-frog scheme defined as follows (Hernquist and Katz, 1989):

$$\begin{aligned} \mathbf{v}_i^{n+1/2} &= \mathbf{v}_i^{n-1/2} + \Delta t\, \mathbf{a}_i^n \\ \mathbf{x}_i^{n+1} &= \mathbf{x}_i^n + \Delta t\, \mathbf{v}_i^{n+1/2} \\ \mathbf{v}_i^{n+1} &= \mathbf{v}_i^{n+1/2} + \frac{1}{2}\Delta t\, \mathbf{a}_i^n \end{aligned} \tag{18}$$

where Δt is the time step subject to the Courant-Friedrichs-Lewy (CFL) condition. In the SPH approach, this condition is imposed by considering the smoothing length as a reference length:

$$\Delta t = \mathrm{CFL} \min_{i=1}^{N} \left(\frac{h_{sm,i}}{c_i + \|\mathbf{v}_i\|} \right) \tag{19}$$

SPH type schemes are generally stable for CFL values: $0 < CFL \leq 0.5$.

3 RESULTS AND DISCUSSION

To check the ability of the HLLC finite volume scheme and the SPH method to reproduce accurate numerical solutions, we apply a series of steady and unsteady flow tests, in which the analytical or experimental solutions are available. Two codes are used in this investigation. It is BASEMENT V2.8 Code (Vetsch et al., 2022) which is based on the finite volume approach. For the SPH approach, we use the code SW-SPHysics 2D V1.0 (Vacondio et al., 2011). We thus make the necessary and appropriate modifications for each test case. In all tests, we admit g = 9.81m/s^2, ρ = 1000 kg/m^3, and a variable time step so that the CFL number is 0.9 in the finite volume method and 0.4 in the SPH method. Both codes have been executed in an Intel(R) Core (TM) i5-10300H CPU @ 2.50GHz with 16.0 GB RAM.

3.1 Typical dam break

This classic benchmark test verifies the shock-capturing ability of numerical schemes. The 1D analytical solution to this

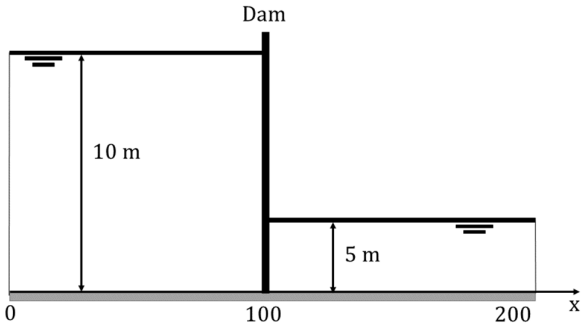


Fig. 5. Initial conditions for the typical dambreak problem.

problem is given by (Gallardo et al., 2007). Consider a smooth horizontal rectangular channel of width $b = 10\,\text{m}$ and length $L = 200\,\text{m}$ (cf. Figure 5). The initial conditions consist of zero discharge along the domain, the water depth is given by:

$$h = \begin{cases} 10\,\text{m} & \text{if } 0 < x \leq 100 \\ 5\,\text{m} & \text{if } x > 100 \end{cases} \quad (20)$$

The problem is subject to the open boundary conditions at the upstream and downstream ends of the channel. The domain is discretized into 11109 triangular cells when using the finite volume method. As for the SPH method, the domain is discretized into 2222 fluid particles and 2211 bed or bottom particles. In this test, we check the influence of the MUSCL reconstruction on the results provided by the SPH method.

The dam placed in the middle of the channel collapses instantly at $t = 0\,s$. The analysis of the Froude number (cf. Figure 6) shows that the present test admits a subcritical flow along the channel. The flow associated with the dambreak generates two waves; a rapidly advancing shock wave that travels downstream and a rarefaction wave propagating upstream. Figure 7 presents the numerical results of both methods after three seconds of the dam failure. The right side represents the space evolution of the specific discharge whereas, the water depth is presented on the left side.

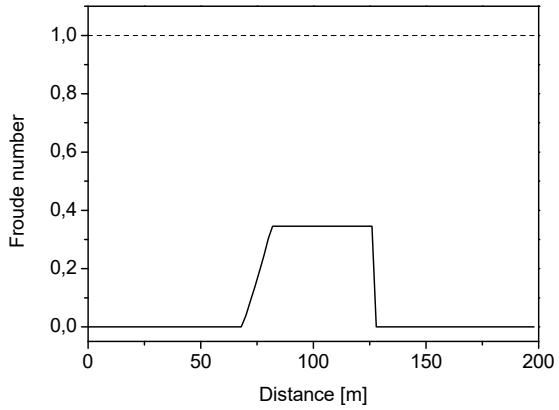


Fig. 6. Froude number variation.

One can notes that both methods are able to produce more accurate shock wave, the SPH method introduces additional viscosity into the rarefaction wave. However, by applying the MUSCL reconstruction, the numerical viscosity level is reduced. Table 1 shows the $L2$ norm of the relative error (Equation (21)) and confirms that both methods give a good correlation with the analytical solution.

$$Er_2 = \sqrt{\sum_{i=1}^{N} \left(\frac{h_a - h_c}{h_a}\right)^2} \quad (21)$$

where; h_a is the analytical solution of the water depth and h_c is the simulated solution.

Hence, for the rest of test cases, we use the SPH method with MUSCL reconstruction. On the other hand, the SPH method is found to exhibit oscillation at the location of the contact discontinuity, where it generates an unphysical non-stationary jump that spoils the solution. This oscillation indicatesthat the numerical instabilities is due to the approximations and assumptions used in the SPH method.

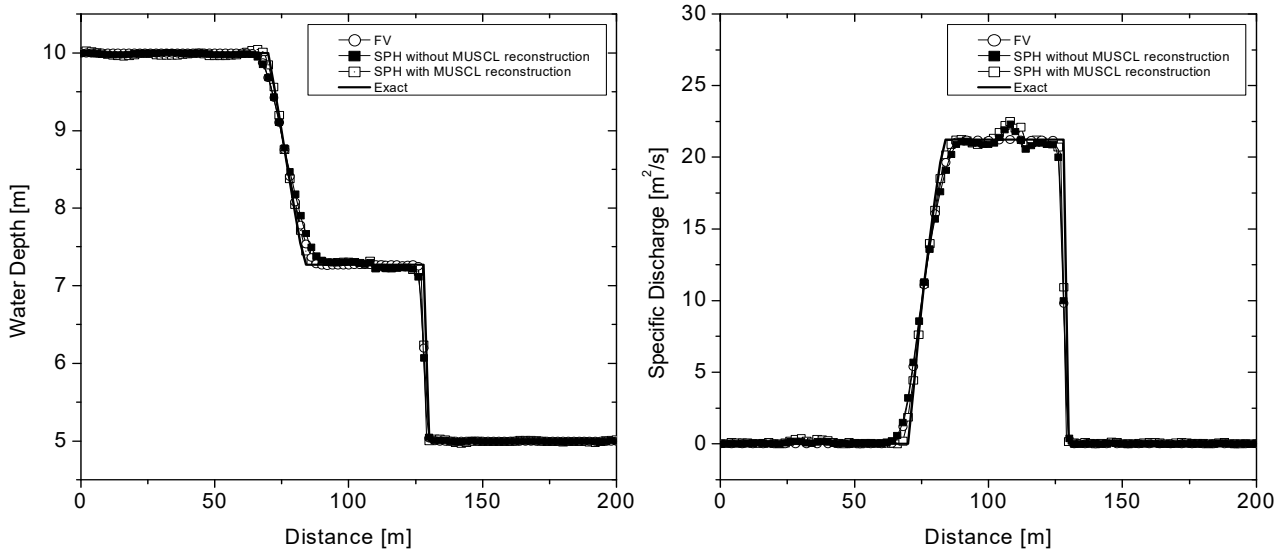


Fig. 7. Numerical results of a typical dambreak: Water depth (left), Specific discharge (right).

Table 1. L2-norm of relative error: case of typical dambreak.

Numerical schemes	*L2* relative errors (%)
FVM	0.16
SPH without MUSCL reconstruction	0.25
SPH with MUSCL reconstruction	0.15

3.2 Dambreak over triangular bump

In this test, the case of a dambreak wave interacting with a triangular obstacle is considered to study the ability of both methods to manage the longitudinal variation of the topography and to control the wetting and drying case. The stability and the precision of the numerical schemes are also checked, in particular at the triangular obstacle. This experiment was conducted at the University of Brussels in Belgium as a reference test (Hiver, 2000). It has been recommended by the European Commission of the CADAM project.

Figure 8 shows the benchmark geometry in detail. The physical model has a length of 38 m and a width of 0.75 m. A dam located at x = 15.5 m divides the domain into a reservoir filled at 0.75 m and a dry floodplain containing a triangular obstacle which has 0.4 m high and 6 m at the base and located at 13 m downstream the dam. Downstream the bump, the water depth is fixed at 0.15 m. Six gauging points (G4, G10, G13, G14, G15, and G20) are respectively installed at 4 m, 10 m,13 m, 14 m, 15 m, and 20 m downstream of the dam. The time simulation is 90 s. Manning's friction coefficient at the channel bottom is 0.0125 $m^{-1/3}s$. Both upstream and downstream boundaries are closed. The computational domain consists of 22079 triangular cells for the 2D finite volume method, while in the SPH model the domain is discretized into 31060 fluid particles and 47151 bed particles.

A sudden and total dambreak at time $t = 0$ s generates initially an expansion wave that propagates upstream and a shock wave that rapidly advances along the channel. Downstream the triangular obstacle, the flow becomes complex and involves multiple interactions between the waves. We can perceive the complexity of the flow in the Figure 9 which shows the evolutions of the dambreak wave along the centerline of the channel at different time. Figure 10 shows a comparison between the predicted water depths and those observed at different measurement points.

The calculation of the mean absolute error MAE (Equation (22)) between the experimental data and numerical solutions is given in Table 2.

$$\mathrm{MAE} = \frac{\sum_{i=1}^{n} |h_e - h_c|}{n} \tag{22}$$

where; h_e is the experimental data of the water depth, h_c is the simulated results, n is the step number.

The analysis shows that both methods are able to simulate water depthsaccurately, especially at the beginning of the simulation. However, the SPH method produces slightly more accurate results at certain gauges (G4, G10, and G15) compared to the finite volume method (cf. Table 2). At gauge G14, both methods underestimate the water depth, though the finite volume method providing abetter result.

Approaching to the closed boundary, at time 5.4 s, one notices an unphysical variation of the water depths which leads to an instability in the numerical schemes (cf. Figure 9). This variation disappears after time, $t = 7.4$ s, in the finite volume approach but increases in the SPH method, which creates a large oscillation at gauge G20 in Figure 10. These oscillations due by the combination of the smooth fluid-fluid interaction. However, the arriving time of the wave is accurately predicted and this is the more important factor in dam-break simulation.

The finite volume method takes 267.38 seconds to achieve the simulation while the SPH method takes about 9 hours. The SWE-SPPhysics code don't use a parallel computing like the CPU-OpenMP adopted in BASEMENT V2.8 which can significantly improve efficiency and thus reduce computation time. However, we are convinced that the simulation time taken by the SWE-SPhysics model will still remain high relative to that of the BASEMENT model because of the number of CFL imposed in the SPH method which equals to the half that in the FV method. This induces a smaller time step and therefore a higher computation time. Moreover, the length of the cell-cell interface in the FV mesh is constant, while SPH approach uses the Newton-Raphson method to update the smoothing length.

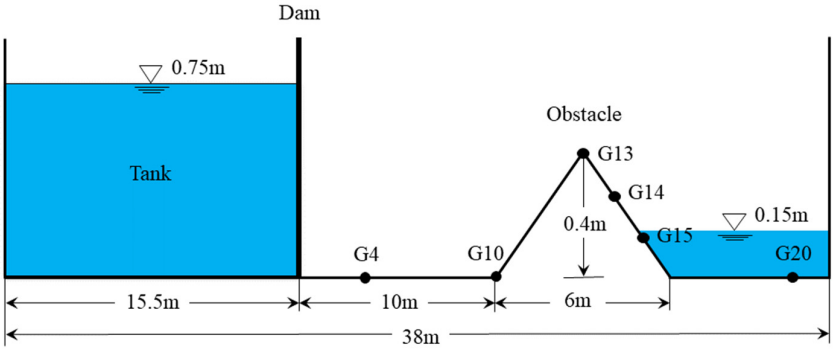


Fig. 8. Physical model of a dambreak on a triangular obstacle.

Table 2. Mean Absolute Error (MAE): case of a dambreak on a triangular bump.

	Mean Absolute Error (MAE)					
	G4	G10	G13	G14	G15	G20
Coordinates (m)	4	10	13	14	15	20
FVM	0.168	0.025	0.010	0.067	0.036	0.023
SPH	0.161	0.022	0.013	0.082	0.025	0.044

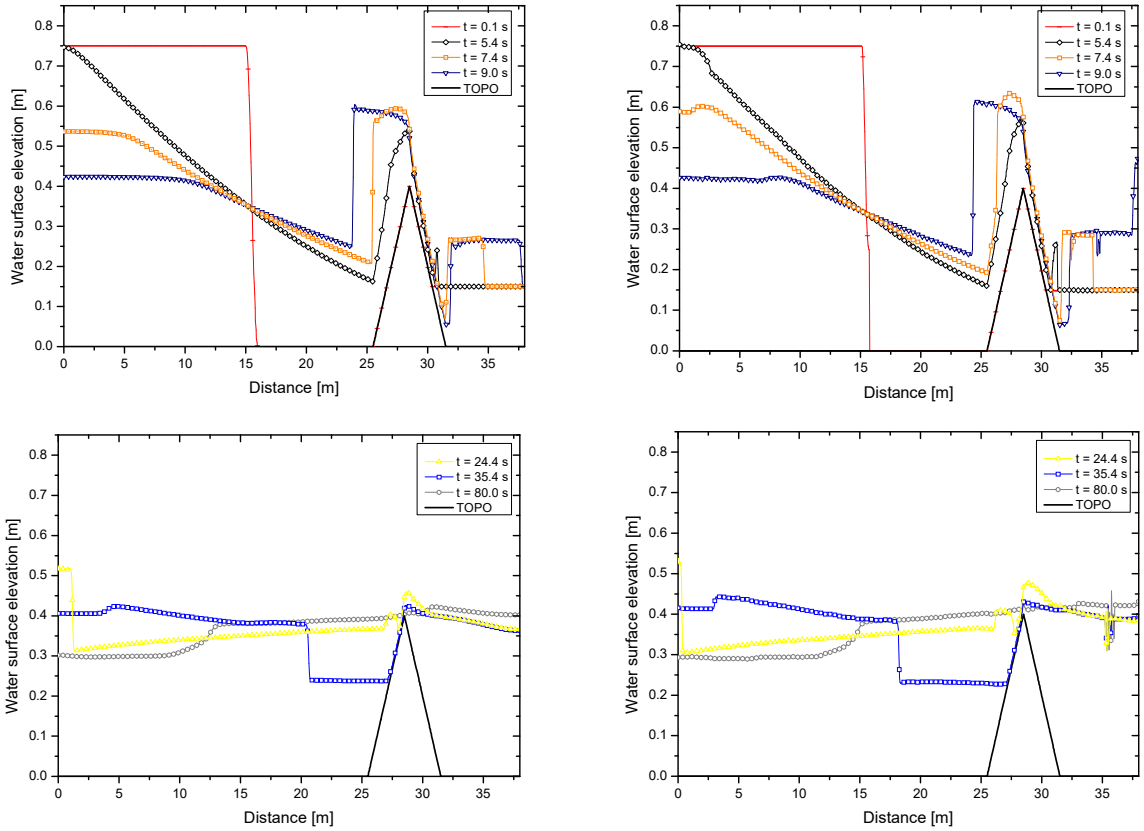


Fig. 9. Temporal evolution of the dam break wave at time t = 0.1, 5.4, 7.4, 9.0, 24.4, 35.4 and 80 s for both methods: (left)FVM; (right) SPH method.

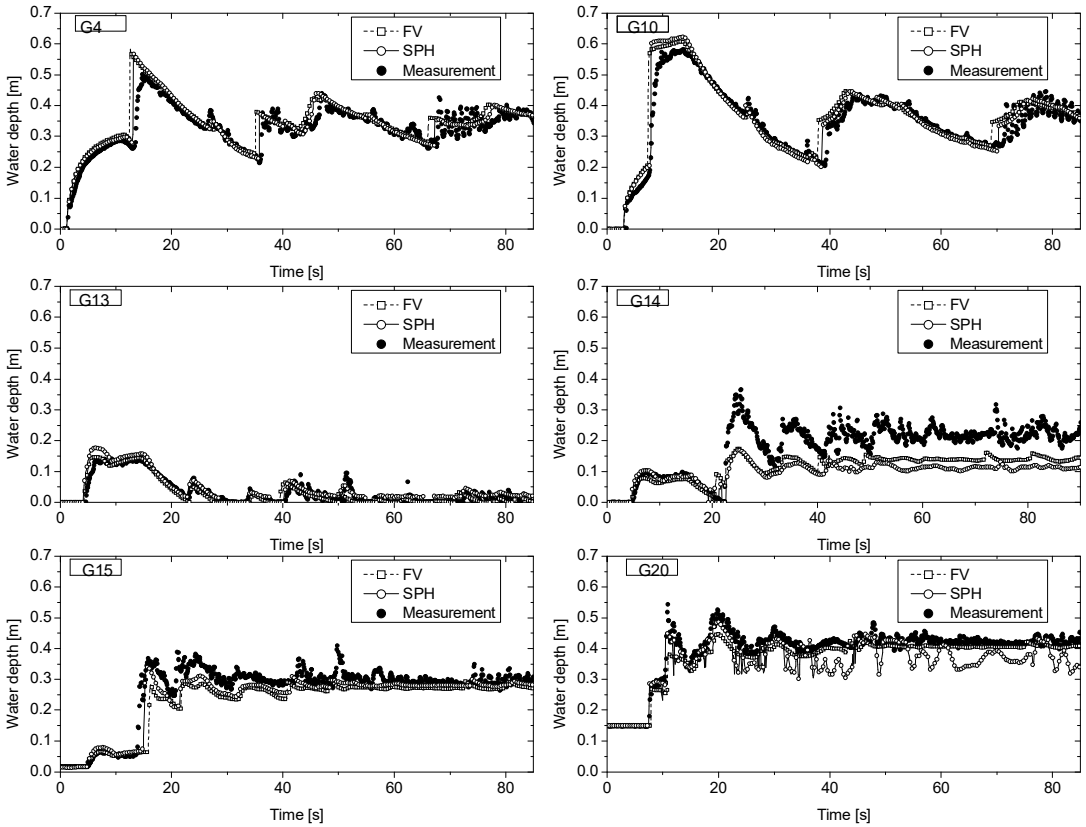


Fig. 10. Calculated and observed water depth.

3.3 Unsteady flow in venturi channel

This test case was originally developed by Bento (Bento Franco, 1996). The aim is to study an unsteady flow due to a dambreak in a venturi channel. The generated dambreak wave is partially reflected by the contraction at the middle of the channel, then undergoes attenuation downstream. This test involves the presence of a shock wave and two types of flow regimes from subcritical to supercritical. Therefore, it is possible to verify the ability of the models to process a complex flow in a 2D domain with a variable width. The geometry of the channel is detailed in Figure 11. It consists of a rectangular and horizontal channel 19.3 m long and 0.5 m wide. A dam is located 6.1 m from the upstream end. 7.7 m downstream of the dam, the channel contracts linearly to reach 0.1 m wide. After the contraction of 1 m in length, the channel returns linearly to its initial width.

Four gauging points distributed along the center line of the channel (G1, G2, G3, and G4) provide the experimental depth, their locations are indicated in Table 3. G1 is located upstream of the dam where an expansion wave occurs and causes a drop in the water depth. G2 is before the contraction where we observe the arrival of a shock wave caused by the dambreak after 3s and later at $t = 7.3$ s we note another abrupt change in the depth coming from a reflected wave produced by contraction. This reflected shock propagates upstream. The G3 measurement point is inside the contraction where a sudden increase in water depth occurs. Finally, G4 is localized after the contraction, in which a small diffracted shock wave is observed, then the water depth tends to stabilize.

Table 3. Coordinates of the gauging points.

Points	G1	G2	G3	G4
X	0.25	0.25	0.25	0.25
Y	5.1	12.2	14.7	16.6

In this test, the initial depth upstream the dam is 0.3m and 0.003m downstream. A wall-closed boundary condition is set at the upstream boundary while the downstream end is considered transmissive. The Manning coefficient is 0.01 $m^{-1/3}s$. The domain is discretized into 17129 triangular cells in the finite volume approach, and 15384 fluid particles and 16212 bed particles in the SPH model. The time simulation is 10s after the instantaneous dambreak. Figure 12 shows a comparison of the experimental data and the numerical results of the temporal evolution of the water depth at the measuring points G1, G2, G3, and G4. The relative errors in the *L2*-norm are presented in Table 6. Considering the *L2*-norm relative error, the finite volume method produces significantly better results than the SPH method (cf. Table 4). The CPU time using the finite volume method (45.08 s) is much lower compared with that of the SPH method (2006.81 s).

Table 4. Relative errors in *L2*-norm: case dambreak in a venturi channel.

	L2 relative errors (%)			
	G1	G2	G3	G4
FVM	1.66	2.71	3.79	3.01
SPH	1.81	3.20	4.04	4.31

Numerical solutions predicted from the HLLC solver satisfactorily reproduce the physical behavior of the dambreak wave, despite some discrepancies comparing to the observed data, namely at G1 and G3 (cf. Figure 12). On the other hand, the SPH method, appears to have difficulty to capturethe flow sharp gradients specially at the contraction. This is resulted in the penetration of fluid particles through the walls. Which leads to the simulation errors in the water depths at G3 and the delay of the arrival time of the shock wave at G4.

5 CONCLUSION

In this study, we were interested in the numerical simulation of some types of two-dimensional, non-stationary free surface flows which are governed by the 2D shallow water equations. In particular, the dambreak case with various configurations which creates a range of flow features such as shock waves, dispersive waves, and hydraulic jumps.

The comparison between two shock-capturing numerical approaches has been investigated. These are the Eulerian HLLC finite volume solver and the Lagrangian Smoothed Particle Hydrodynamics (SPH) method. The main difference consists of the fact that the finite volume method is a mesh-based on the mesh while the SPH method is a meshless particleapproach.

Various unsteady two-dimensional flow tests were performed which provide insight into the accuracy, stability and robustness of both methods in the presence of more complex waves.

The comparison with the analytical solution and the available experimental measurements shows that both methods arerobust enough to predict the numerical solution and capable to simulate this type of flow, especially the arrival time of the wave. The first case is a purely academic test of a typical frictionless dambreak. Thus, it was found that the MUSCL reconstruction improve the quality of the numerical solutions in the SPH formulation. We have also checked the impact of the vertical and the horizontal variation of the geometry with friction in the second and the third test, respectively.

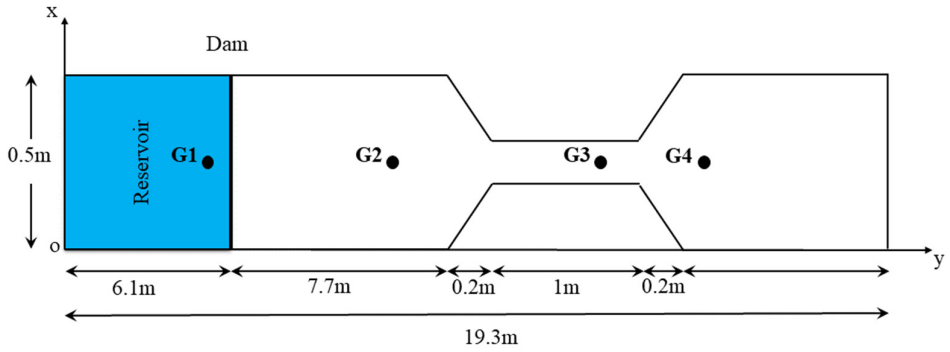


Fig. 11. Geometry of the venturi channel.

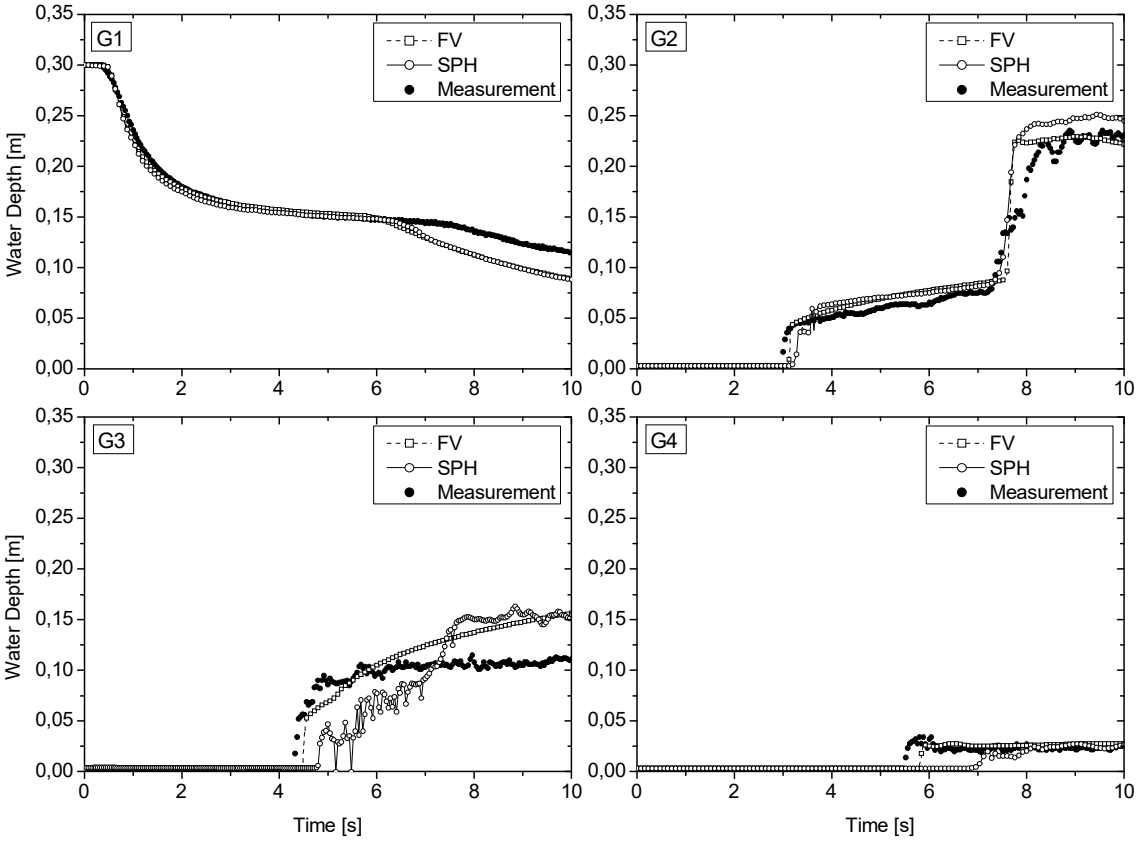


Fig. 12. Comparison between experimental data and numerical results 10 s after the dambreak.

Although an artificial viscosity was used, the SPH method behaves badly with abrupt changes of properties (density, water depth or pressure) through a contact discontinuity, which is translated by non-physical and non-stationary jump. Alternatively, it is also affected by the choice of the kernel function, the smoothing length and the time step. In addition, the SPH model has difficulty in maintaining the balance between the fluxes and the source term of the bed due to the accumulation of the interpolation errors.

According to the MAE and MSE error values, the HLLC finite volume scheme has the advantage in terms of accuracy, stability, effectiveness and computation time thanks to the parallel computing and the CPU-OpenMP technique adopted in the BASEMENT model.

To improve the performance of the SPH method, it is necessary to perform a parametric study to select the optimum conditions which gives competing results. We should then apply it in real cases such as flooding with inflow and outflow boundary conditions.

Acknowledgement. The authors would like to thank anonymous Reviewers for taking the time and effort necessary for the manuscript examination. We sincerely appreciate all valuable comments and suggestions, which helped us to improve the quality of the paper.

REFERENCES

Abbott, M.B., McCowan, A.D., Warren, I.R., 1984. Accuracy of short-wave numerical models. Journal of Hydraulic Engineering, 110, 10, 1287–1301. https://doi.org/10.1061/(asce)0733-9429(1984)110:10(1287)

Alcrudo, F., Garcia-Navarro, P., Saviron, J.-M., 1992. Flux difference splitting for 1D open channel flow equations. International Journal for Numerical Methods in Fluids, 14, 9, 1009–1018. https://doi.org/10.1002/fld.1650140902

Ata, R., Soulaïmani, A., 2005. A stabilized SPH method for inviscid shallow water flows. International Journal for Numerical Methods in Fluids, 47, 2, 139–159. https://doi.org/10.1002/fld.801

Bento Franco, A., 1996. Modelacao computacional e experimental de escoamentos provocados por roturas de barragens. PhD Thesis. Universidade Tecnica de Lisboa, Portugal.

Benz, W., 1990. Smooth particle hydrodynamics: A review. In: The Numerical Modelling of Nonlinear Stellar Pulsations. Springer, Dordrecht, pp. 269–288. https://doi.org/10.1007/978-94-009-0519-1_16

Bermudez, A., Vazquez, M.E., 1994. Upwind methods for hyperbolic conservation laws with source terms. Computers & Fluids, *23*, 8, 1049–1071.

BMT & WBM, 2014. TUFLOW FV User Manual: Flexible Mesh Modelling. In: Build 2014.01 (Issue Build, p. 298). https://downloads.tuflow.com/_archive/TUFLOW_FV/Manual/TUFLOW_FV_User_Manual_2020.pdf

Bonet, J., Lok, T.S.L., 1999. Variational and momentum preservation aspects of Smooth Particle Hydrodynamic formulations. Computer Methods in Applied Mechanics and Engineering, 180, 1–2, 97–115. https://doi.org/10.1016/S0045-7825(99)00051-1

Brunner, G.W., 2018. HEC-RAS River Analysis System: Verification and Validation Tests. RD-52., Davis, California.

Bunya, S., Kubatko, E.J., Westerink, J.J., Dawson, C., 2009. A wetting and drying treatment for the Runge-Kutta discontinuous Galerkin solution to the shallow water equations. Computer Methods in Applied Mechanics and Engineering, 198, 17–20, 1548–1562. https://doi.org/10.1016/j.cma.2009.01.008

Chaudhry, M.H., 2008. Open-Channel Flow. 2nd Edition. Springer, US. https://doi.org/10.1007/978-0-387-68648-6

Cunge, J.A., Holly, F.M., Verwey, A., 1980. Practical Aspects of Computational River Hydraulics. Pitman Publishing Ltd, London, 17 CUN, 420.

Danish Hydraulic Institute DHI., 2014. MIKE FLOOD 1D-2D Modelling User Manual. 162 p. https://manuals.mikepoweredbydhi.help/2021/Water_Resources/MIKE_FLOOD_UserManual.pdf

Delestre, O., Lucas, C., Ksinant, P.A., Darboux, F., Laguerre, C., Vo, T.N.T., James, F., Cordier, S., 2016. SWASHES: A compilation of shallow water analytic solutions for hydraulic and environmental studies. International Journal for Numerical Methods in Fluids, 74, 3, 229–230. https://doi.org/10.1002/fld.3865

Deltares systems, 2019. SOBEK Hydrodynamics, Rainfall Runoff and Real Time Control-User Manual (1.00). Deltares. https://www.deltares.nl

Domínguez, J.M., Fourtakas, G., Altomare, C., Canelas, R.B., Tafuni, A., García-Feal, O., Martínez-Estévez, I., Mokos, A., Vacondio, R., Crespo, A.J.C., Rogers, B.D., Stansby, P.K., Gómez-Gesteira, M., 2021. DualSPHysics: from fluid dynamics to multiphysics problems. Computational Particle Mechanics, 9, 5, 867–895. https://doi.org/10.1007/s40571-021-00404-2

Edwards, M.G., 2006. The dominant wave-capturing flux: A finite-volume scheme without decomposition for systems of hyperbolic conservation laws. Journal of Computational Physics, 218, 1, 275–294. https://doi.org/10.1016/j.jcp.2006.02.005

Gallardo, J.M., Parés, C., Castro, M., 2007. On a well-balanced high-order finite volume scheme for shallow water equations with topography and dry areas. Journal of Computational Physics, 227, 1, 574–601. https://doi.org/10.1016/j.jcp.2007.08.007

Gingold, R.A., Monaghan, J.J., 1977. Smoothed particle hydrodynamics: theory and application to non-spherical stars. Monthly Notices of the Royal Astronomical Society, 181, 3, 375–389. https://doi.org/10.1093/mnras/181.3.375

Glaister, P., 1988. Solution approchée d'un probléme de riemann pour les equations de saint-venant. Journal of Hydraulic Research, 26, 3, 293–306. https://doi.org/10.1080/00221688809499213

Godunov, S., 1959. Finite difference method for numerical computation of discontinuous solutions of the equations of fluid dynamics. Matematicheskii Sbornik, 47, 89, 3, 271–306. https://hal.archives-ouvertes.fr/hal-01620642

Gu, S., Zheng, X., Ren, L., Xie, H., Huang, Y., Wei, J., Shao, S., 2017. SWE-SPHysics simulation of dam break flows at South-Gate Gorges Reservoir. Water (Switzerland), 9, 6, 387. https://doi.org/10.3390/w9060387

Harten, A., Lax, P.D., van Leer, B., 1983. On upstream differencing and Godunov-type schemes for hyperbolic conservation laws. SIAM Review, 25, 1, 35–61. https://doi.org/10.1137/1025002

Hérault, A., Vicari, A., Del Negro, C., 2008. A SPH thermal model for the cooling of a lava lake. In: Proceedings of the 3th SPHERIC Workshop (Lausanne).

Hernquist, L., Katz, N., 1989. TREESPH - A unification of SPH with the hierarchical tree method. The Astrophysical Journal Supplement Series, 70, 419. https://doi.org/10.1086/191344

Hervouet, J.M., Ata, R., 2017. User manual of opensource software TELEMAC-2D User manual of opensource software TELEMAC-2D V7P2. http://www.opentelemac.org/

Hirsch, C., 1988. Numerical Computation of Internal and External Flows. Vol. 1: Fundamentals of Numerical Discretization. John Wiley & Sons, Ltd.

Hiver, J.M., 2000. Adverse-slope and slope (bump). Concerted Action on Dam Break Modelling: Objectives. Project Report, Test Cases, Meeting Proceedings, 400.

Komaei, S., Bechteler, W., 2004. An improved, robust implicit solution for the two dimensional shallow water equations on unstructured grids. River Flow, 1065–1072. https://doi.org/10.1201/b16998-137

LeVeque, R.J., 2002. Finite Volume Methods for Hyperbolic Problems. Cambridge University Press. https://doi.org/10.1017/cbo9780511791253

Li, H., Liu, R.X., 2001. The discontinuous Galerkin finite element method for the 2D shallow water equations. Mathematics and Computers in Simulation, 56, 3, 223–233. https://doi.org/10.1016/S0378-4754(01)00277-4

LISFLOOD-FP Developers, 2020. LISFLOOD-FP 8.0 hydrodynamic model (8.0). Zenodo. https://doi.org/10.5281/ZENODO.4073011

Liu, G.R., Liu, M.B., 2003. Smoothed particle hydrodynamics. In: Smoothed Particle Hydrodynamics. WORLD SCIENTIFIC. https://doi.org/10.1142/5340

Lucy, L.B., 1977. A numerical approach to the testing of the fission hypothesis. The Astronomical Journal, 82, 1013. https://doi.org/10.1086/112164

Mandli, K.T., Ahmadia, A.J., Berger, M., Calhoun, D., George, D.L., Hadjimichael, Y., Ketcheson, D.I., Lemoine, G.I., LeVeque, R.J., 2016. Clawpack: Building an open source ecosystem for solving hyperbolic PDEs. PeerJ Computer Science, 8, e68. https://doi.org/10.7717/peerj-cs.68

Mingham, C.G., Causon, D.M., 1998. High-resolution finite-volume method for shallow water flows. Journal of Hydraulic Engineering, 124, 6, 605–614. https://doi.org/10.1061/(asce)0733-9429(1998)124:6(605)

Molls, T., Chaudhry, M.H., 1995. Depth-averaged open-channel flow model. Journal of Hydraulic Engineering, 121, 6, 453–465. https://doi.org/10.1061/(asce)0733-9429(1995)121:6(453)

Monaghan, J.J., 1994. Simulating free surface flows with SPH. Journal of Computational Physics, 110, 2, 399–406. https://doi.org/10.1006/jcph.1994.1034

Monaghan, J.J., 2005. Smoothed particle hydrodynamics. Reports on Progress in Physics, 68, 8, 1703–1759. IOP Publishing. https://doi.org/10.1088/0034-4885/68/8/R01

Nujić, M., 1995. Développement de schémas numériques performants non oscillatoires pour les écoulements à surface libre. Journal of Hydraulic Research, 33, 1, 101–111. https://doi.org/10.1080/00221689509498687

Osher, S., Solomon, F., 1982. Upwind difference schemes for hyperbolic systems of conservation laws. Mathematics of Computation, 38, 158, 339. https://doi.org/10.2307/2007275

Ríha, J., Duchan, D., Zachoval, Z., Erpicum, S., Archambeau, P., Pirotton, M., Dewals, B., 2019. Performance of a shallow-water model for simulating flow over trapezoidal broad-crested weirs. Journal of Hydrology and Hydromechanics, 67, 4, 322–328. https://doi.org/10.2478/johh-2019-0014

Roberts, S., Nielsen, O., Gray, D., Sexton, J., 2015. ANUGA User Manual. Geoscience Australia, May, jg.

Rodriguez-Paz, M., Bonet, J., 2005. A corrected smooth particle hydrodynamics formulation of the shallow-water equations. Computers and Structures, 83, 17–18, 1396–1410. https://doi.org/10.1016/j.compstruc.2004.11.025

Roe, P.L., 1981. Approximate Riemann solvers, parameter vectors, and difference schemes. Journal of Computational Physics, 43, 2, 357–372. Academic Press. https://doi.org/10.1016/0021-9991(81)90128-5

Saint-Venant, A.J.-C., 1871. Théorie du mouvement non-permanent des eaux, avec application aux crues des rivieres eta l'introduction des marées dans leur lit. CR Acad. Sci. Paris, 73, 147–154, 5.

Shepard, D., 1968. A two-dimensional interpolation function for irregularly-spaced data. In: Proceedings of the 23rd ACM National Conference ACM 1968, pp. 517–524. https://doi.org/10.1145/800186.810616

Steger, J.L., Warming, R.F., 1981. Flux vector splitting of the inviscid gasdynamic equations with application to finite-difference methods. Journal of Computational Physics, 40, 2, 263–293. https://doi.org/10.1016/0021-9991(81)90210-2

Toro, E.F., 2001. Shock-Capturing Methods for Free Surface Shallow Flows. John Wiley & Sons, Ltd. https://www.wiley.com/en-us/Shock+Capturing+Methods+for+Free+Surface+Shallow+Flows-p-9780471987666

Toro, E.F., Spruce, M., Speares, W., 1994. Restoration of the contact surface in the HLL-Riemann solver. Shock Waves, 4, 1, 25–34. https://doi.org/10.1007/BF01414629

Vacondio, R., Rogers, B.D., Stansby, P.K., 2011. Smoothed particle hydrodynamics: Approximate zero-consistent 2-D boundary conditions and still shallow-water tests. International Journal for Numerical Methods in Fluids, 69, 1, 226–253. https://doi.org/10.1002/fld.2559

Vetsch, D., Siviglia, A., Bürgler, M., Caponi, F., Ehrbar, D., Facchini, M., Faeh, R., Farshi, D., Gerber, M., Gerke, E., Kammerer, S., Koch, A., Mueller, R., Peter, S., Rousselot, P., Vanzo, D., Veprek, R., Volz, C., Vonwiller, L., Weberndorfer, M., 2022. System Manuals of BASEMENT, Version 2.8.2 Laboratory of Hydraulics, Glaciology and Hydrology (VAW). ETH Zurich. http://www.basement.ethz.ch

Yang, Q., Wu, W., Wang, Q.J., Vaze, J., 2022. A 2D hydrodynamic model-based method for efficient flood inundation modelling. Journal of Hydroinformatics, 24, 5, 1004–1019. https://doi.org/10.2166/hydro.2022.133

Yoon, T.H., Kang, S.-K., 2004. Finite volume model for two-dimensional shallow water flows on unstructured grids. Journal of Hydraulic Engineering, 130, 7, 678–688. https://doi.org/10.1061/(ASCE)0733-9429(2004)130:7(678)

Zhao, D.H., Shen, H.W., Tabios, G.Q., Lai, J.S., Tan, W.Y., 1994. Finite-volume two-dimensional unsteady-flow model for river basins. Journal of Hydraulic Engineering, 120, 7, 863–883. https://doi.org/10.1061/(asce)0733-9429(1994)120:7(863)

Zoppou, C., Roberts, S., 1999. Catastrophic collapse of water supply reservoirs in urban areas. Journal of Hydraulic Engineering, American Society of Civil Engineers, 125, 7, 686–695.

Received 5 November 2022
Accepted 15 February 2023